Interaction-based ion selectivity exhibited by self-assembled, cross-linked zwitterionic copolymer membranes

Samuel J. Lounder^a and Ayse Asatekin^{a,1}

^aDepartment of Chemical and Biological Engineering, Tufts University, Medford, MA 02155

Edited by Howard A Stone, Princeton University, Princeton, NJ, and approved May 18, 2021 (received for review January 4, 2021)

Water filtration membranes with advanced ion selectivity are urgently needed for resource recovery and the production of clean drinking water. This work investigates the separation capabilities of cross-linked zwitterionic copolymer membranes, a self-assembled membrane system featuring subnanometer zwitterionic nanochannels. We demonstrate that selective zwitterion-anion interactions simultaneously control salt partitioning and diffusivity, with the permeabilities of NaClO₄, NaI, NaBr, NaCl, NaF, and Na₂SO₄ spanning roughly three orders of magnitude over a wide range of feed concentrations. We model salt flux using a one-dimensional transport model based on the Maxwell-Stefan equations and show that diffusion is the dominant mode of transport for 1:1 sodium salts. Differences in zwitterion-Cl⁻ and zwitterion-F⁻ interactions granted these membranes with the ultrahigh Cl^-/F^- permselectivity ($P_{Cl}/P_{F^-} = 24$), enabling high fluoride retention and high chloride passage even from saline mixtures of NaCl and NaF.

membranes | self-assembly | ion separation | synthetic ion channel | biomimetic

embranes with advanced ion selectivity could provide a sustainable technical solution to global resource shortages. For example, dangerously high concentrations of fluoride in available drinking water sources affects many communities, resulting in widespread, debilitating illnesses such as fluorosis (1, 2). Membranes with enhanced chloride/fluoride selectivity could protect these communities from fluorosis without necessitating highpressure filtration or remineralization of the drinking water (2, 3). Limited geological reserves of lithium and uranium pose a major challenge to sustainable lithium battery production and nuclear power generation, respectively (4). Membranes capable of selective ion retention could enrich aqueous feedstocks with desired ions, enabling efficient capture of precious metals (5). Current synthetic membranes separate solutes by size and charge differences (6, 7), limiting their use in advanced ion separations such as these. As such, the design of synthetic membrane filters with targeted ion selectivity represents a crucial challenge for addressing global resource shortages.

Biological ion channels (BICs) exhibit exquisite ion selectivity that can inspire novel membranes capable of precise ion separations. Potassium channels permeate potassium >10,000 times faster than sodium, despite the sub-Å size difference between these equally charged ions (8). While synthetic membranes separate ions primarily by size and charge differences (6, 7), BICs rely on interactive functional groups that line the walls of nanopores (6, 9). The favorability and strength of these interactions control ion partitioning and diffusion rate, providing a powerful mechanism for separating similarly sized ions (6, 9). Crucially, BIC pore diameters are comparable to or slightly smaller than the hydrated diameter of the target ion (6, 9). This nanoconfinement forces ions to interact with the functional groups lining the pores, greatly amplifying selectivity (6, 9).

Numerous approaches have attempted to translate this separation mechanism to synthetic systems, including the use of supramolecular assemblies (10), carbon nanotubes (11, 12), and graphene oxide laminates (13). These various approaches face severe manufacturing challenges (6, 14), however, and the use of polymeric materials is preferrable due to low cost and simple scale-up (6). For example, block copolymers (BCPs) have been used to fabricate ultrafiltration (UF) membranes with controlled pore wall functionality (15), leading to tunable selectivity through solute-membrane interactions (16, 17). However, the relatively large size of BCP membrane pores (>2 to 3 nm) limits its use for ion separations. Membranes formed from packed arrays of random copolymer micelles have demonstrated selectivity based on solute charge (9) and aromaticity (18), but the pore size of these membranes is also too large to separate salt ions. It has been shown that the transport properties of ion exchange membranes are affected by the compatibility between the ions and fixed charge groups (19, 20), but this approach has not been utilized to design advanced membrane filters.

Random zwitterionic amphiphilic copolymers (r-ZACs) are random/statistical copolymers that combine zwitterionic and hydrophobic repeat units. Strong interactions between zwitterions (ZIs) drive the formation of a bicontinuous network of zwitterionic nanochannels surrounded by a hydrophobic nanophase (21-24). Thin film composite (TFC) membranes are prepared by coating a thin (~1 µm) copolymer layer onto porous supports, a simple and scalable membrane fabrication process. During aqueous filtration, the zwitterionic domain functions as a network of

Significance

The separation of ions is challenging yet crucial for providing access to safe water resources as well as recovering valuable ions from water and wastewater. Yet, membranes rarely exhibit selectivity between ions of similar charge and size. We demonstrate that membranes, prepared by a fully scalable method that uses self-assembling zwitterionic copolymers, exhibit exceptional selectivity between salt anions of similar size and charge. We show that this unusual capability is derived from selective zwitterion-ion interactions occurring within the nanochannels, similarly to biological ion channels. We further demonstrate these membranes exhibit Cl⁻/F⁻ permselectivity more than twice the values reported in previous studies, with applications in treating groundwater streams to prevent fluorosis and in wastewater treatment.

Author contributions: S.J.L. and A.A. designed research; S.J.L. performed research; S.J.L. and A.A. analyzed data; and S.J.L. and A.A. wrote the paper.

Competing interest statement: A.A. owns a minor equity in and serves as the Senior Scientific Advisor of ZwitterCo. Inc., which was the lead institution in the NSF grant IIP-1843847 that partially funded this work. ZwitterCo also holds a license from Tufts University to commercialize the technology described in this manuscript.

This article is a PNAS Direct Submission.

Published under the PNAS license

¹To whom correspondence may be addressed. Email: Ayse.Asatekin@tufts.edu.

This article contains supporting information online at https://www.pnas.org/lookup/suppl/ doi:10.1073/pnas.2022198118/-/DCSupplemental.

Published September 7, 2021.

hydrophilic nanochannels for the transport of water and small solutes. For a broad range of copolymer compositions (21, 22, 25), r-ZAC membranes possess pores that are too large to achieve ion

Recently, we developed r-ZAC membranes with subnanometer channels and exceptional mono/divalent ion selectivity (26). These TFC membranes are prepared using an r-ZAC that contains crosslinkable allyl groups (Fig. 14). After membrane fabrication, we extensively cross-link the hydrophobic domain by photopolymerization. This prevents the zwitterionic nanochannels from swelling water, resulting in a smaller effective pore size during aqueous filtration (26). Highly cross-linked r-ZAC membranes (ZAC-X) have an effective pore diameter of only ~0.9 nm, based on the 99.7% retention of sucrose (SI Appendix, Fig. S1) (26), and achieved one of the highest Cl⁻/SO₄²⁻ selectivities reported (26). The small pore size of ZAC-X is essential for the observed selectivity because uncross-linked r-ZAC membranes with larger pores exhibited relatively limited ion selectivity.

ZAC-X presents a unique self-assembled membrane system featuring subnanometer nanochannels lined with abundant ioninteractive ZI groups (Fig. 1B). In this work, we investigate the ion selectivity of ZAC-X during pressure-driven filtration over a wide range of feed concentrations. We show that favorable ZIanion interactions lead to enhanced salt partitioning and permeation rate, whereas ZI-cation interactions play a limited role (Fig. 1C). We employ a Maxwell-Stefan (MS) modeling approach to show that 1:1 sodium salts permeate via diffusion only. Differences in ZI-Cl⁻ and ZI-F⁻ interactions granted ZAC-X with ultrahigh Cl⁻/F⁻ selectivity, enabling the treatment of water sources with high fluoride content. This work offers a scalable approach for the design of ion-selective membrane filters.

Results and Discussion

Polymer Synthesis and Membrane Manufacture. The cross-linkable r-ZAC, poly(allyl methacrylate-r-sulfobetaine methacrylate) (P(AMAr-SBMA)) containing 47 weight(wt)% SBMA (Fig. 1A), was synthesized using Activators ReGenerated by Electron Transfer-Atom Transfer Radical Polymerization (ARGET-ATRP). This copolymer composition was selected as it was expected to microphase separate into a bicontinuous morphology leading to highly permeable yet stable selective layers (21, 22). The copolymer composition closely matched the monomer ratios in the reaction mixture despite the reaction being stopped at $\sim 10\%$ conversion, implying a roughly random sequence of monomers. Using gel permeation chromatography (GPC), we determined that the number-averaged molecular weight was 1.8×10^5 Da with a dispersity of 5.4. The large dispersity was due to the presence of a high molecular weight fraction, which likely formed due to slight intermolecular chain cross-linking (SI Appendix, Fig. S2) (27). This copolymer was rod coated onto a commercial UF membrane support (PS35, Solecta) and dried using a heat gun, resulting in TFC membranes with an ~450-nm thick selective layer (Fig. 1A). TFC membranes were then soaked in a solution of photoinitiator in isopropyl alcohol, which swells the hydrophobic nanodomain but not the zwitterionic nanochannels. Exposure to ultraviolet (UV) light for 20 min led to the polymerization of the allyl groups of AMA, reducing the nanochannel diameter to <1.0 nm (26). The resultant membrane, ZAC-X, exhibited a water permeance of $0.37 \text{ L} \cdot \text{m}^{-2} \cdot \text{hr}^{-1} \cdot \text{bar}^{-1}$, in agreement with previous studies (26).

Rejection of Sodium and Chloride Salts. Water and small solutes permeate r-ZAC TFC membranes through a network of selfassembled zwitterionic nanochannels (Fig. 1B) (21, 22, 25). Unlike previous r-ZAC membranes, however, ZAC-X possesses exceptionally narrow nanochannels (<1.0 nm). Due to confinement, we expect that permeating ions are forced to intimately interact with the ZI groups lining the nanochannel wall of ZAC-X. This would provide a clear mechanism to achieve interactionbased selectivity, since interactions are known to simultaneously affect partitioning and diffusivity (19). Experimental (28-30) and simulation (31) studies indicate that SB groups preferentially bind with weakly hydrated anions (e.g., CIO_4^-) over strongly hydrated anions (e.g., SO_4^{-2}). SB-cation interactions are comparatively weaker (28), although they can still disrupt ZI-ZI pairs (32).

To study the effect of SB-anion and SB-cation interactions on membrane selectivity, we measured the rejection of various

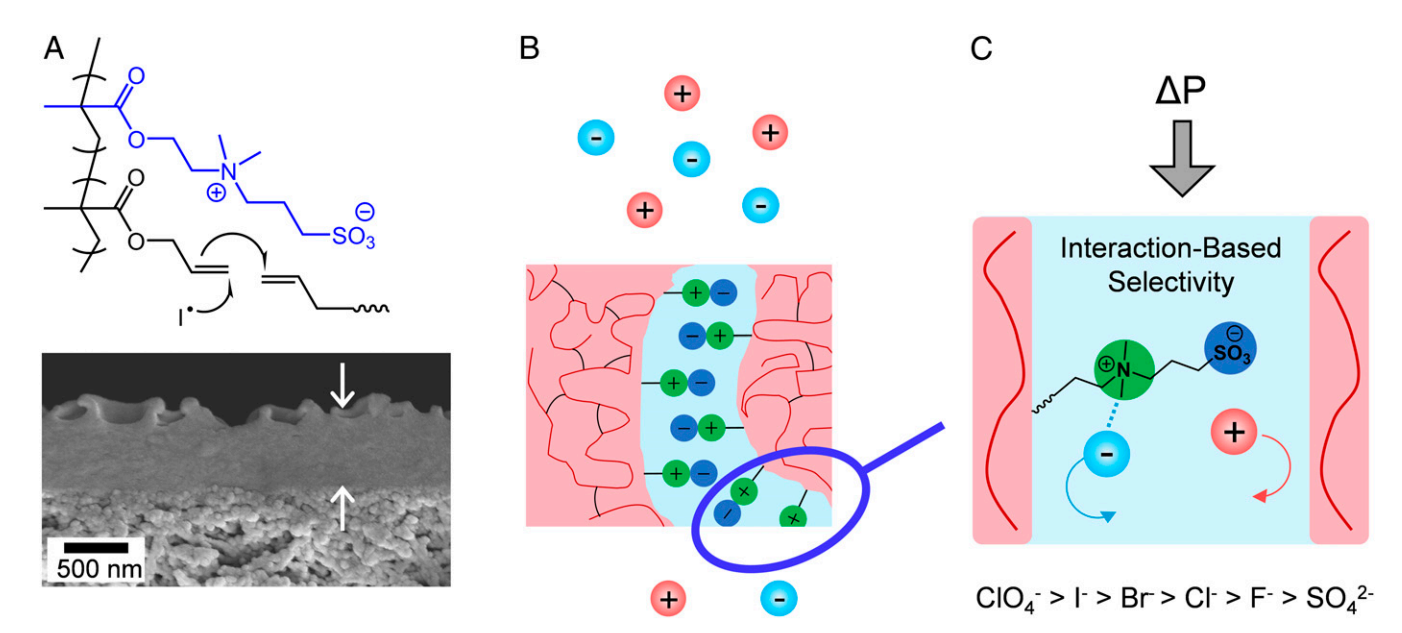
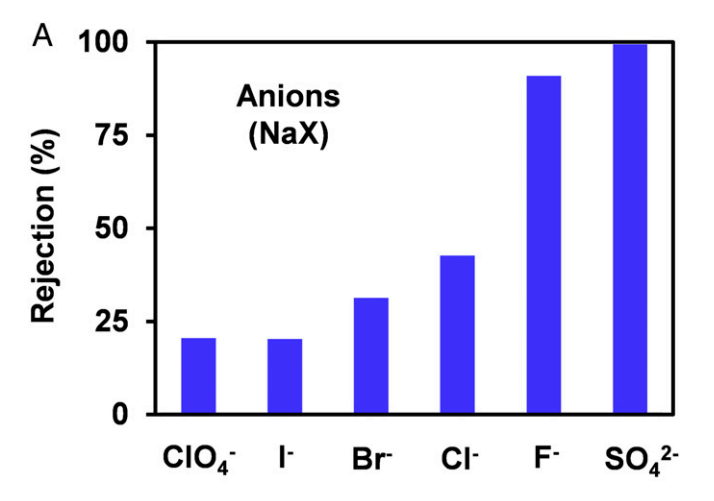


Fig. 1. (A, Top) Chemical structure of the cross-linkable r-ZAC, poly(allyl methacrylate-r-sulfobetaine methacrylate) (P(AMA-r-SBMA)). (Bottom) FESEM crosssectional image of a TFC membrane. The dense top layer is the cross-linkable r-ZAC on the support. (B) Illustration of cross-linked r-ZAC nanostructure. The hydrophobic domain (red) surrounds the zwitterionic nanochannels (blue), which permeate water and certain ions. The hydrophobic domain is chemically cross-linked to reduce the effective pore size to <1.0 nm (26). (C) Schematic showing the ZI-ion interactions occurring during pressure-driven filtration within the zwitterionic nanochannel. Favorable ZI-anion interactions enable higher permeation rates due to enhanced salt partitioning. These membranes enable selective separations during pressure-driven filtration, a highly scalable mode of operation.

sodium (NaX) and chloride (MCl) salts at 20 mM feed concentration and 250 psi operating pressure (Fig. 2 A and B). Rejection varied broadly among sodium salts with different anions (NaX). The variation was unusually wide among anions with the same valence, from 21% for NaClO₄ to 91% for NaF. This clearly demonstrates the unusual ability of cross-linked r-ZAC membranes to separate ions based on their chemical structure. The rejection sequence followed NaClO₄ ~ NaI < NaBr < NaCl < NaF < Na₂SO₄ (Fig. 2A). This order closely follows ZI–anion interactions, with lower salt rejections corresponding to more favorable ZI–anion interactions. The retention of Na₂SO₄ was extremely high (99.4%), likely because SB–SO₄²⁻ interactions are highly unfavorable (30).

In contrast, the rejection of chloride salts with different cations (MCl) appeared to be most heavily influenced by the cation charge and size, with the larger divalent cations Ba²⁺ and Mg²⁺ rejected more than monovalent cations Cs⁺, Na⁺, and Li⁺ (Fig. 2B). The rejections of Ba²⁺ and Mg²⁺ are comparable with that of similarly sized neutral solutes (~90%) (26), implying a size exclusion mechanism. This also explains the similar retentions of Cs⁺, Na⁺, and Li⁺, because noninteractive membranes also demonstrate similar rejections of salts containing these cations



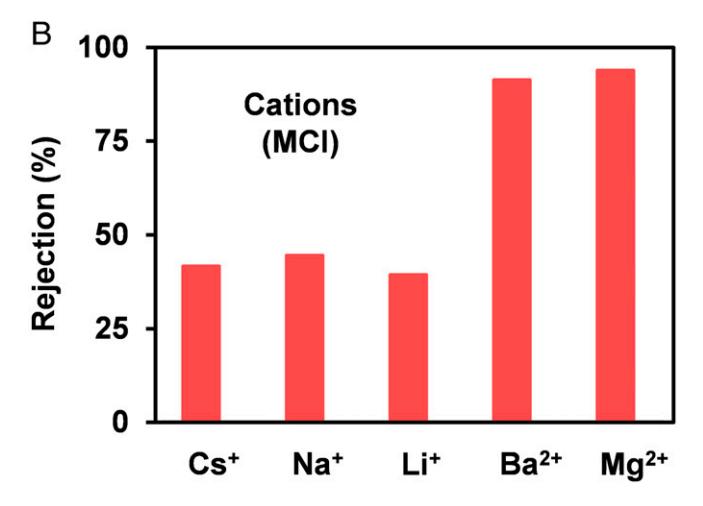


Fig. 2. Rejection of various sodium (NaX) and chloride (MCI) salts at 250 psi pressure. (A) Rejection of NaX with various anions. Rejection increases with increasing anion hydration strength (*Left* to *Right*), which correlates closely with SB–anion interaction propensity. (B) Rejection of MCI with various cations. Rejection is not clearly determined by cation hydration strength (increasing *Left* to *Right*). Higher rejections are observed for divalent cations than monovalent cations.

(33, 34). These results suggest that the weaker SB–cation interactions (28, 30) have limited impact on selectivity. The rejection of perchlorate salts (CsClO₄, NaClO₄, and LiClO₄) showed a similar trend, with monovalent cation species having little effect on salt rejection (*SI Appendix*, Fig. S3).

Transport Modeling. To study the underlying mechanisms that govern the selectivity of these membranes, we modeled the permeation of sodium salts using the MS equations (35–37). The MS equations, derived from irreversible thermodynamics, provide a comprehensive description of diffusion while also accounting for convection through frame of reference corrections and friction coupling (36, 37). This framework has successfully modeled multicomponent diffusion in numerous membrane systems, including reverse osmosis, UF, ion exchange, pervaporation, and gas permeation membranes (35). We utilized the integrated MS equations derived by Paul (36) and further adapted the model to describe the transport of charged species under the constraint of electroneutrality (*SI Appendix*). Simplifying assumptions allowed us to concisely express salt flux in terms of the diffusive and convective contributions:

$$\frac{N_s w_m \delta}{\Delta C_s} = P_s + u_w \overline{c_s} \varepsilon_s \frac{\delta}{\Delta C_s}.$$
 [1]

The left-hand side of Eq. 1, termed "normalized salt flux," is the product of superficial salt flux (N_s) and the copolymer weight fraction for the swollen membrane (w_m) normalized by diffusion driving force $(\Delta C_s/\delta)$, where $\Delta C_s = C_{s,\text{Feed}} - C_{s,\text{Permeate}}$, and δ is the effective membrane thickness). The first term on the right-hand side of Eq. 1 is salt permeability (P_s) , which is the diffusion contribution to the normalized salt flux. The second term is convective flux $(u_w \overline{c_s} \varepsilon_s)$, where u_w is superficial water velocity, $\overline{c_s}$ is average salt concentration in the membrane, and ε_s is the salt friction coupling coefficient) normalized by diffusion driving force $(\Delta C_s/\delta)$. Eq. 1 deconvolutes diffusive and convective transport, the relative contributions of which can be determined by filtering salt solutions at varying u_w (SI Appendix). The diffusive component can be further analyzed to calculate permeability (P_s) :

$$P_s = D_s K_s. ag{2}$$

 D_s describes the diffusivity of both the anion and the cation of the salt because both species must diffuse together to maintain electroneutrality in the overall-neutral zwitterionic nanochannels. K_s is the salt partition coefficient and quantifies the molar concentration of salt in the membrane relative to that of the adjacent bulk solution:

$$K_s = \frac{c_s}{c_{s,b}}. [3]$$

Where c_s and $c_{s,b}$ are molar salt concentration in the membrane and bulk phases, respectively. K_s is affected by membrane–ion interactions (Fig. 1C), ion dehydration, steric exclusion, and electroneutrality (38). For 1:1 salts, an equal number of cations and anions must partition into the overall-neutral zwitterionic nanochannels to maintain electroneutrality. The analogously defined water sorption coefficient (K_w) is given by the following:

$$K_w = \frac{c_w}{c_{wh}}.$$
 [4]

Where c_w and $c_{w,b}$ are molar water concentration in the membrane and bulk phases, respectively. For simplicity, it is generally assumed that water absorbed by the membrane has the same density as bulk water (39). To analyze transport through the ZAC-X membrane using this model, we filtered sodium salts at 20 mM

feed concentration with varying transmembrane pressures and plotted normalized salt flux against water velocity (Fig. 3). According to Eq. 1, the convective contribution to the normalized salt flux increases with water velocity, whereas the diffusion contribution (permeability, P_s) remains constant. For NaClO₄, NaI, NaBr, NaCl, and NaF, we observed no increase in normalized salt flux with u_w . This indicates that diffusion is the dominant transport mechanism for these salts.

Na₂SO₄ was the only salt that showed significant contributions from both diffusion and convection, with normalized salt flux increasing with water velocity (Fig. 3 and SI Appendix). The diffusive flux of this salt was extremely low in comparison to other salts, leading to high retention (99.4%). Convective permeation may be significant only for a small portion of membrane area that is less tightly cross-linked. This contribution would be not visible for the other sodium salts (NaClO₄, NaI, NaBr, NaCl, and NaF) due to their greater permeability.

Sorption and Permselectivity. To determine the mechanism for the observed selectivity, we measured the salt partition coefficient (K_s) of the sodium salts via salt uptake experiments (Fig. 4A). Salt uptake increased linearly with external salt concentration for 20 to 500 mM (SI Appendix, Figs. S5 and S6), similar to other uncharged polymers (39). K_s exactly followed the order of ZIanion interaction propensity, indicating that favorable ZI-anion interactions lead to enhanced salt partitioning. This result explains why lower retention/faster permeation rates were observed for salts with more favorable ZI-anion interactions (Figs. 2 and 3). Notably, the copolymer demonstrated preferred sorption of NaClO₄ and NaI over water, with K_{NaClO4} and K_{NaI} exceeding the analogously defined water sorption coefficient (K_w , Fig. 4A). This preference for salt sorption over water sorption is rarely observed in membrane systems (39) and likely suggests extensive interactions. Furthermore, such high salt partitioning relative to water could only be possible if a large portion of the partitioned ions were favorably interacting with the ZIs. Indeed, NaClO₄ was absorbed so extensively that it was enriched in the copolymer phase relative to the bulk solution ($K_{NaClO4} = 1.45$).

To further investigate selectivity, we measured the permeability (Ps, Eq. 1) of NaClO4, NaI, NaBr, NaCl, NaF, and Na₂SO₄ over a wide range of feed concentrations (Fig. 4B). For lower salt concentrations (20 to 60 mM), we observed $P_{NaClO4} \approx$ $P_{NaI} > P_{NaBr} > P_{NaCl} > P_{NaF} >> P_{Na2SO4}$. With the exception of

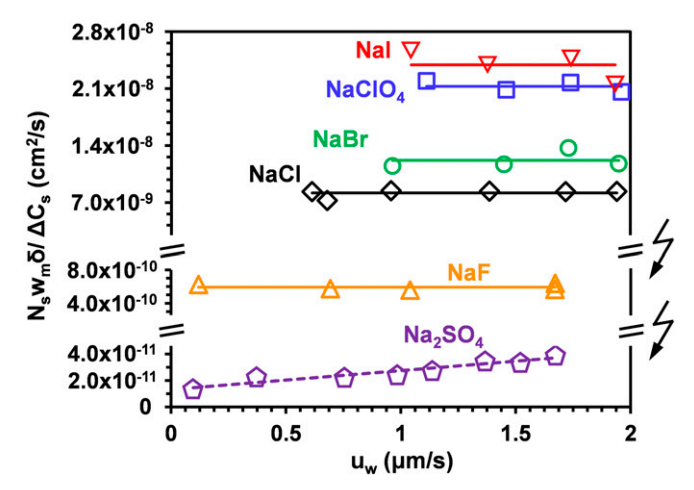


Fig. 3. Normalized salt flux $(N_s w_m \delta/\Delta C_s)$ versus water velocity (u_w) for NaClO₄, NaI, NaBr, NaCl, NaF, and Na₂SO₄ at 20 mM feed concentration. Model fit (Eq. 1) reveals that convection is negligible for all salts except Na₂SO₄, which had important contributions from both diffusion and convection.

 $P_{NaClO4} \approx P_{NaI}$, this trend exactly follows the order of ZI-anion interaction propensity. While the effects of size exclusion are difficult to isolate, this result illustrates that excellent interactionbased permselectivity was accessed by our system. For instance, the permeability of NaClO₄ was 39 times greater than that of NaF at 20 mM feed concentration, despite the <0.2 Å size difference between ClO₄⁻ and F⁻ (40).

Salt permeability appeared to increase with feed concentration for all salts except NaClO₄ (Fig. 4B and SI Appendix, Table S4). This reflects a slight increase in salt diffusivity, because the partition coefficients remained constant with external salt concentration for 20 to 500 mM (SI Appendix, Figs. S5 and S6). For uncharged polymers, salt diffusivity generally remains constant with feed concentration (39). Poly(ZIs) are known to be salt responsive, however, undergoing conformational changes through the antipolyelectrolyte effect (30). This phenomenon may have led to small molecular rearrangements within the nanochannels, causing salt diffusivity and permeability to slightly increase with feed concentration. The exact mechanism underlying this rearrangement is still unclear, however, because stronger ZI-anion interactions did not correspond to a greater dependence of P_s on feed concentration. Interestingly, the order of permeability changed to $P_{NaI} > P_{NaClO4} \approx P_{NaBr} > P_{NaCl} > P_{NaF} >> P_{Na2SO4}$ at the highest feed concentration (500 mM), despite the dependence of P_s on feed concentration being relatively weak. This change in the P_s sequence occurred because P_s increased for all salts except NaClO₄.

Salt diffusivities (D_s) were calculated using the measured values for K_s and P_s (Eq. 2, Fig. 4C). In contrast to partitioning, we did not expect diffusivity to be enhanced by favorable interactions. For a ZI-complexed ion to execute a diffusion hop, it must first break the transient bond with the ZI (Fig. 1C). This process contributes to the diffusion energy barrier (7). The strong dependence of K_s and P_s on ZI-anion interaction propensity suggests that extensive ZI-ion interactions occur within the nanochannels. Therefore, favorable ZI-anion interactions were expected to result in lower diffusivity. Interestingly, we observed $D_{NaBr} \sim D_{NaCl} > D_{NaI} > D_{NaClO4} \sim D_{NaF} >> D_{Na2SO4}$ over the full range of feed concentrations (Fig. 4C). The anions of the first four salts in this sequence, I⁻, Br⁻, Cl⁻, and ClO₄⁻, are similarly sized. Therefore, this result suggests that Br and Cl⁻ had similar binding strengths, I⁻ had slightly stronger binding than Br^- and Cl^- , and ClO_4^- had stronger binding than I^- (31). This result agrees well with the salt partition coefficients (K_s) , because the high values of K_{NaI} and especially K_{NaClO4} suggest extensive and favorable ZI-anion interactions. The lower diffusivities of NaF and Na₂SO₄ were likely due to greater anion size.

Chloride-Fluoride Separation. Despite the similar size and equal charge of Cl⁻ and F⁻, NaCl permeated much faster than NaF through ZAC-X due to favored ZI-Cl⁻ interactions (Fig. 4). This selectivity is ideally suited for the removal of fluoride from drinking water. Excessive NaCl rejection necessitates remineralization, adding to separation cost and complexity (2, 3). ZAC-X is also highly resistant to membrane fouling. Indeed, ZAC-X, similar to other r-ZAC-based membranes, exhibits no measurable irreversible fouling when exposed to various foulants, fully retaining its performance even with challenging feeds (26). This is another key performance feature for this application (2), as well as industrial water treatment and reuse applications where selective ion removal is desired.

While these results are promising, membrane selectivity often declines with complex feeds (9). We therefore filtered equimolar mixtures of NaCl/NaF (Fig. 5A) to confirm that NaCl does not reduce the Cl⁻/F⁻ selectivity inferred from the single-salt filtration experiments. Fig. 5A shows normalized fluoride flux $(N_F w_m \delta/\Delta C_F)$ and fluoride rejection versus ionic strength (I) for NaF-only (single) and equimolar NaCl/NaF (mixed) solutions. Normalized

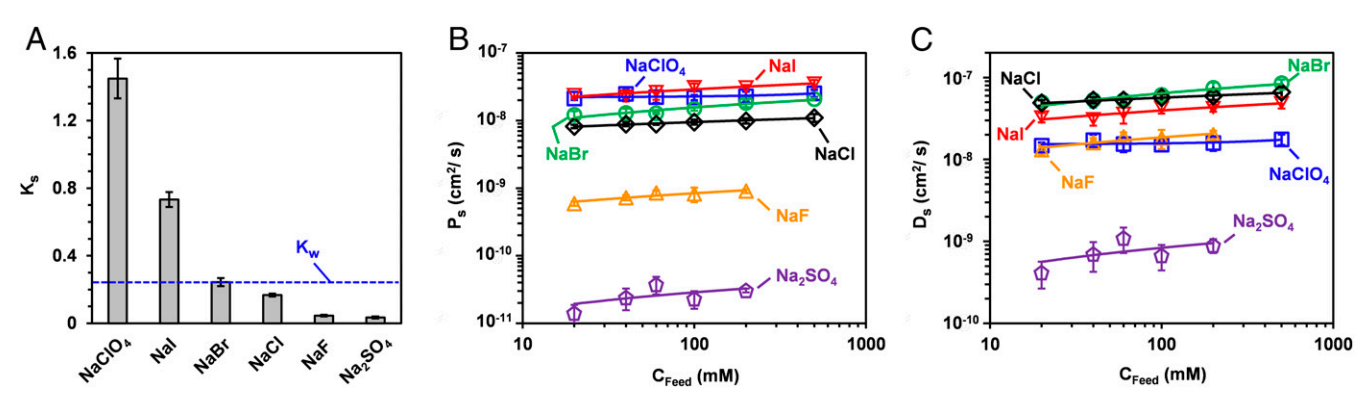


Fig. 4. Partition coefficient (K_s, A), permeability (P_s, B), and diffusivity (D_s, C) of sodium salts. The water sorption coefficient (K_w) is also included in A. Greater partitioning and permeability generally corresponded to more favorable ZI-anion interactions, while diffusivity depended on interaction strength as well as anion size.

fluoride flux and fluoride rejection were identical for the singlesalt and mixed-salt solutions of matching I, indicating that chloride had no apparent effect on fluoride transport beyond contributing to the total ionic strength. The total salinity of the feed solutions ranged from slightly brackish (500 parts per million [ppm]) to heavily brackish (3,000 ppm), demonstrating that ZAC-X can successfully filter fluoride from realistic drinking water sources at a reasonable operating flux (6 to 7 L \cdot m⁻² \cdot hr⁻¹). Fluoride rejection ranged between 92.5 to 88.1%, high enough to reduce the fluoride content to below the World Health Organization (WHO) limit (1.5 ppm) for problematic water sources from the United States, Turkey, Germany, China, and India (2).

The Cl⁻/F⁻ permselectivity of ZAC-X, defined as P_{NaCl}/P_{NaF} , greatly surpassed that of state-of-the-art polyamide TFC (3, 41–46) and anion exchange (47-49) membranes (Fig. 5B). For instance, ZAC-X achieved a maximum mixed-salt Cl⁻/F⁻ permselectivity of 24, compared to only 4.4 for the polyamide membranes. ZAC-X also doubled the in-operation Cl⁻/F⁻ selectivity of previously reported membranes in terms of Cl⁻/F⁻ separation factor (SF) (SI Appendix, Fig. S9). The uncross-linked r-ZAC membrane demonstrated much lower Cl⁻/F⁻ permselectivity than ZAC-X due to low retention of both NaCl and NaF (Fig. 5B and SI Appendix, Table S6). This result illustrates that both selective ZI-anion interactions and extremely small subnanometer pores are needed to achieve exceptional ion selectivity. Interestingly, ZAC-X demonstrated greater selectivity in mixed- versus single-salt mode, whereas the opposite was observed for the polyamide membranes (Fig. 5B). This enhanced mixed-salt selectivity was due to the lower retention of Cl⁻ during mixed-salt filtration (SI Appendix, Table S6). While the underlying mechanism is not yet clear, it is consistent with previous studies of membranes with nanoscale, functionalized pores (9, 18). These results motivate further study of the synergistic use of nanoconfinement and chemical interactions to achieve previously inaccessible membrane separations (6).

Conclusions

This work demonstrates that cross-linked r-ZAC membranes provide a powerful platform for the scalable manufacture of nanostructured membrane filters with advanced ion selectivity. Favorable ZI-anion interactions led to enhanced salt partitioning, with the partition coefficients of NaClO₄ and NaI greatly exceeding the analogously defined water sorption coefficient. Permeability mostly followed the order of ZI-anion interaction propensity, spanning roughly three orders of magnitude for NaClO₄, NaI, NaBr, NaCl, NaF, and Na₂SO₄ over a wide range of feed concentrations. Different ZI-Cl⁻ and ZI-F⁻ interactions granted the membranes with exceptional Cl-/F- permselectivity and SFs, enabling high fluoride retention with NaCl/NaF mixtures ranging from slightly brackish to heavily brackish salinity levels. Uncrosslinked r-ZAC membranes with larger pores demonstrated much lower Cl⁻/F⁻ permselectivity, illustrating that confinement was essential for the observed separation performance. These results

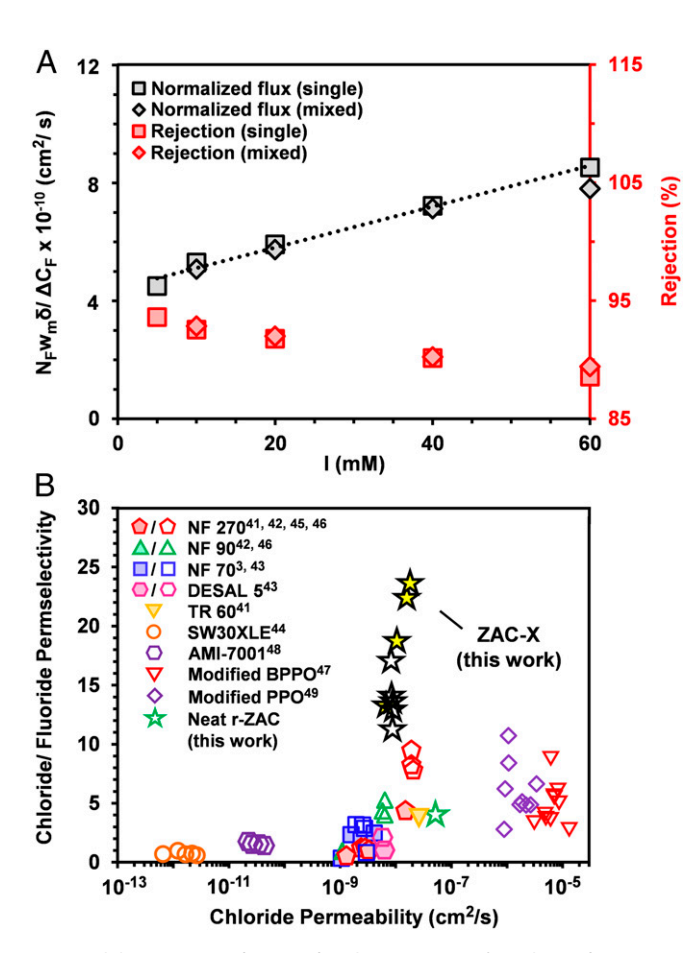


Fig. 5. (A) Normalized fluoride flux ($N_F W_m \delta / \Delta C_F$, Left axis) and fluoride rejection (Right axis) for NaF solutions (single) and equimolar mixtures of NaCl/ NaF (mixed) versus ionic strength (I). Pressure was adjusted to maintain 6 to 7 L · m⁻² · hr⁻¹ · bar⁻¹ operating flux. (B) Cl⁻/F⁻ permselectivity (P_{NaCl}/P_{NaF}) versus CI⁻ permeability for ZAC-X, uncross-linked r-ZAC, polyamide TFC (3, 41-46), and anion exchange (47-49) membranes. Closed and open symbols correspond to mixed- and single-salt permselectivity, respectively. Permeability was determined using equations relevant to each experimental condition (reference SI Appendix for further details). Data are tabulated in SI Appendix, Table S6.

underscore the potential for cross-linked r-ZAC membranes to perform advanced ion separations at the commercial scale (50), providing an efficient and green strategy for addressing crucial separations such as selective fluoride removal.

Materials, detailed experimental procedures, derivation of the MS modeling approach, and tabulated data are reported in SI Appendix.

Copolymer Synthesis. The cross-linkable r-ZAC was synthesized using methods described in previous work (26). In brief, P(AMA-r-SBMA) was synthesized by ARGET-ATRP of AMA and SBMA, which preserved the allylic C = C groups for future cross-linking (Fig. 1A).

GPC. Copolymer molecular weight was determined using a Shimadzu GPC system equipped with a PSSPolymer PFG column, guard column, and refractive index detectors. The mobile phase was a solution of trifluoroethyl potassium salt/trifluoroethanol (0.05 M) eluted at 1.0 mL/min. Poly(methyl methacrylate) standards were used for the calibration (ReadyCal Kit).

Membrane Preparation/Characterization. To prepare TFC membranes (26), we coated a 3 wt/volume(vol)% solution of P(AMA-r-SBMA) in trifluoroethanol onto a commercial support (PS35, Solecta). The solvent was evaporated using a heat gun (Sparkfun), leading to TFC membranes with a dense ~450-nm P(AMA-r-SBMA) selective layer (Fig. 1A). After cutting membrane disks and measuring initial permeance and rejections, we equilibrated the disks with a 3 wt/vol% solution of photoinitiator in isopropanol and shined UV light for 20 min to cross-link the hydrophobic domain. This reduced the nanochannel size to <1.0 nm (26), enabling enhanced ZI-ion interactions due to confinement. TFC membrane morphology was characterized using a Zeiss Supra55 VP field emission scanning electron microscope (FESEM). To prepare FESEM samples, membranes were freeze fractured in liquid nitrogen, mounted, and sputter coated with Au/Pd.

Membrane Testing. Filtration experiments were performed on 4.7-cm diameter membrane disks using stainless steel stirred cells (HP 4750, Sterlitech) stirred at 1,000 rpm and pressurized to 20 to 400 psi. For permeance measurements, we applied a known transmembrane pressure (ΔP) and tracked permeate flux over time. For single-salt rejection measurements, we loaded 125 mL feed solution, filtered >6 mL, and then collected the next permeate fraction for analysis. Salt concentration was measured using a conductivity meter (high range, VWR). Rejection of species i (Ri) was determined by the following:

$$R_i = 100\% \left(1 - \frac{C_{i,P}}{C_{i,F}}\right),$$
 [5]

where $C_{i,P}$ and $C_{i,F}$ are permeate and feed concentrations of i, respectively. Single-salt filtration was performed at a range of pressure differences. In NaCl/NaF mixed-salt filtration experiments, pressure was adjusted to maintain 6 to 7 L · m⁻² · hr⁻¹ operating flux. We measured fluoride and chloride concentrations using SPADNS fluoride concentration kit (Hach), conductivity measurements, and Kohlrausch's equation (SI Appendix).

- 1. M. Mohapatra, S. Anand, B. K. Mishra, D. E. Giles, P. Singh, Review of fluoride removal from drinking water. J. Environ. Manage. 91, 67-77 (2009).
- 2. J. Shen, A. Schäfer, Removal of fluoride and uranium by nanofiltration and reverse osmosis: A review, Chemosphere 117, 679-691 (2014).
- A. Lhassani, M. Rumeau, D. Benjelloun, M. Pontie, Selective demineralization of water by nanofiltration application to the defluorination of brackish water. Water Res. 35, 3260-3264 (2001).
- 4. D. S. Sholl, R. P. Lively, Seven chemical separations to change the world. Nature 532,
- 5. A. Razmjou, M. Asadnia, E. Hosseini, A. Habibnejad Korayem, V. Chen, Design principles of ion selective nanostructured membranes for the extraction of lithium ions. Nat. Commun. 10, 5793 (2019).
- 6. I. Sadeghi, P. Kaner, A. Asatekin, Controlling and expanding the selectivity of filtration membranes. Chem. Mater. 30, 7328-7354 (2018).
- 7. R. Epsztein, R. M. DuChanois, C. L. Ritt, A. Noy, M. Elimelech, Towards single-species selectivity of membranes with subnanometre pores. Nat. Nanotechnol. 15, 426-436
- 8. D. A. Doyle et al., The structure of the potassium channel: Molecular basis of K+ conduction and selectivity. Science 280, 69-77 (1998).
- 9. I. Sadeghi, J. Kronenberg, A. Asatekin, Selective transport through membranes with charged nanochannels formed by scalable self-assembly of random copolymer micelles. ACS Nano 12, 95-108 (2018).

Cl⁻/F⁻ permselectivity was calculated using equations relevant to each experimental condition, classified into single-salt filtration (3, 42, 43), concentrationdriven diffusion (44, 48), mixed-salt filtration (3, 41, 43, 45, 46), and anion exchange membranes operated under an applied electric field (47, 49) (reference SI Appendix for further details). CI-/F- SF was defined as follows:

$$SF = \frac{100\% - R_{Cl^-}}{100\% - R_{F^-}}.$$
 [6]

Preparation of Cross-Linked Copolymer Films. Cross-linked copolymer films 30 to 300 μm in thickness were prepared by drying a 3 wt/vol% solution of copolymer/trifluoroethanol on a glass plate. The films were soaked in a 3 wt/vol% solution of photoinitiator in isopropanol and exposed to UV light for 20 min. Cross-linking was confirmed by attenuated total reflectance-Fourier transform infrared spectroscopy performed on both sides of the UVcured films (SI Appendix, Fig. S4).

Measurement of Parameters for MS Equations. Membrane weight fraction (w_m) and water sorption coefficient (K_w) were determined by water uptake measurements using cross-linked copolymer films (39) (SI Appendix):

$$w_m = \frac{1}{1 + w_{\rm up}},\tag{7}$$

$$K_{w} = \frac{W_{\text{up}}}{W_{\text{up}} + \frac{\rho_{w}}{\rho_{p}}}.$$
 [8]

Where $w_{\rm up}$ is water uptake, defined as the mass of absorbed water normalized by the mass of dry polymer (SI Appendix), ρ_{w} is the density of water, and ρ_p is the estimated density of the dry polymer (1.29 g/cm³, SI Appendix). K_s was determined by measuring the moles of salt (n_s) absorbed by polymer films of known dry film mass ($m_{\rm dry}$) that were equilibrated with salt solutions of known concentration ($c_{s,b}$). We then fit $n_s w_m \rho / m_{dry}$ versus c_{sb} with straight lines of zero y-intercept and used the slope to calculate K_s , assuming the volumes of dry copolymer and water are additive and neglecting the effect of salt on copolymer density (SI Appendix):

$$K_{s} = \frac{d\left(\frac{n_{s}w_{mp}}{m_{dry}}\right)}{dc_{sb}}.$$
 [9]

Where ρ is the estimated density of the water-swollen polymer (1.17 g/cm³, SI Appendix).

Data Availability. All study data are included in the article and/or SI Appendix.

ACKNOWLEDGMENTS. We gratefully acknowledge financial support from NSF Grants CBET-1553661 and IIP-1843847 (latter led by ZwitterCo, Inc.), Department of Energy Grant DE-DEFE003185 (led by ZwitterCo, Inc.), and the 2020 to 2021 Environmental Research Fellowship offered by Tufts University's Institute of the Environment. FESEM images were collected by Microvision Laboratories, Inc. We thank Solecta for donating support membranes and ZwitterCo for performing GPC. A.A. thanks Chris Drover for helpful conversations. S.J.L. thanks Abey Klotz for useful discussions.

- 10. Y.-x. Shen, P. O. Saboe, I. T. Sines, M. Erbakan, M. Kumar, Biomimetic membranes: A review. J. Membr. Sci. 454, 359-381 (2014).
- 11. F. Fornasiero et al., Ion exclusion by sub-2-nm carbon nanotube pores. Proc. Natl. Acad. Sci. U.S.A. 105, 17250-17255 (2008).
- 12. H. Li, J. S. Francisco, X. C. Zeng, Unraveling the mechanism of selective ion transport in hydrophobic subnanometer channels. Proc. Natl. Acad. Sci. U.S.A. 112, 10851-10856 (2015)
- 13. N. Song et al., A review of graphene-based separation membrane: Materials, characteristics, preparation and applications, Desalination 437, 59-72 (2018).
- 14. D. M. Stevens, J. Y. Shu, M. Reichert, A. Roy, Next-generation nanoporous materials: Progress and prospects for reverse osmosis and nanofiltration. Ind. Eng. Chem. Res. **56**, 10526–10551 (2017).
- 15. Y. Zhang et al, Fit-for-purpose block polymer membranes molecularly engineered for water treatment. npj Clean Water 1, 1-4 (2017).
- 16. Z. Zhang et al., Chemically tailored multifunctional asymmetric isoporous triblock terpolymer membranes for selective transport. Adv. Mater. 32, e1907014 (2020).
- 17. A. M. Bush et al., Tunable mesoporous films from copolymers with degradable side chains as membrane precursors. J. Membr. Sci. 567, 104-114 (2018).
- 18. I. Sadeghi, A. Asatekin, Membranes with functionalized nanopores for aromaticitybased separation of small molecules. ACS Appl. Mater. Interfaces 11, 12854-12862 (2019).

- Y. Ji, H. Luo, G. M. Geise, Effects of fixed charge group physicochemistry on anion exchange membrane permselectivity and ion transport. *Phys. Chem. Chem. Phys.* 22, 7283–7293 (2020).
- T. Luo, S. Abdu, M. Wessling, Selectivity of ion exchange membranes: A review. J. Membr. Sci. 555, 429–454 (2018).
- P. Bengani, Y. Kou, A. Asatekin, Zwitterionic copolymer self-assembly for fouling resistant, high flux membranes with size-based small molecule selectivity. J. Membr. Sci. 493, 755–765 (2015).
- P. Bengani-Lutz, E. Converse, P. Cebe, A. Asatekin, Self-assembling zwitterionic copolymers as membrane selective layers with excellent fouling resistance: Effect of Zwitterion chemistry. ACS Appl. Mater. Interfaces 9, 20859–20872 (2017).
- M. Ehrmann, J. C. Galin, B. Meurer, Statistical N-butyl acrylate sulfopropyl betaine copolymers. 3. domain size determination by solid-state NMR-spectroscopy. *Macro-molecules* 26, 988–993 (1993).
- T. Y. Wu, F. L. Beyer, R. H. Brown, R. B. Moore, T. E. Long, Influence of Zwitterions on thermomechanical properties and morphology of acrylic copolymers: Implications for electroactive applications. *Macromolecules* 44, 8056–8063 (2011).
- P. Bengani-Lutz, R. D. Zaf, P. Z. Culfaz-Emecen, A. Asatekin, Extremely fouling resistant zwitterionic copolymer membranes with ~1 nm pore size for treating municipal, oily and textile wastewater streams. J. Membr. Sci. 543, 184–194 (2017).
- S. J. Lounder, A. Asatekin, Zwitterionic ion-selective membranes with tunable subnanometer pores and excellent fouling resistance. *Chem. Mater.* 33, 4408–4416 (2021).
- R. París, J. L. de la Fuente, Bulk atom transfer radical polymerization of allyl methacrylate. J. Polym. Sci. A Polym. Chem. 43, 2395–2406 (2005).
- P. Di Profio et al., Effects of headgroup structure on the incorporation of anions into sulfobetaine micelles. Kinetic and physical evidence. Langmuir 14, 2662–2669 (1998).
- L. Marte et al., Specific anion binding to sulfobetaine micelles and kinetics of nucleophilic reactions. J. Phys. Chem. B 111, 9762–9769 (2007).
- T. Wang, X. Wang, Y. Long, G. Liu, G. Zhang, Ion-specific conformational behavior of polyzwitterionic brushes: Exploiting it for protein adsorption/desorption control. *Langmuir* 29, 6588–6596 (2013).
- D. P. Santos, R. L. Longo, Molecular dynamics simulations of specific anion adsorption on sulfobetaine (SB3-14) micelles. J. Phys. Chem. B 120, 2771–2780 (2016).
- Q. Shao, S. Jiang, Molecular understanding and design of zwitterionic materials. Adv. Mater. 27, 15–26 (2015).
- Y. Liang et al., Polyamide nanofiltration membrane with highly uniform subnanometre pores for sub-1 Å precision separation. Nat. Commun. 11, 2015 (2020).
- A. Somrani, A. H. Hamzaoui, M. Pontie, Study on lithium separation from salt lake brines by nanofiltration (NF) and low pressure reverse osmosis (LPRO). *Desalination* 317, 184–192 (2013).

- R. Krishna, J. A. Wesselingh, The Maxwell-Stefan approach to mass transfer. Chem. Eng. Sci. 52, 861–911 (1997).
- D. R. Paul, Reformulation of the solution-diffusion theory of reverse osmosis. J. Membr. Sci. 241, 371–386 (2004).
- Y. Roy, J. H. Lienhard, On the presence of solute-solvent transport coupling in reverse osmosis. J. Membr. Sci. 611. 118272 (2020).
- A. R. Crothers, R. M. Darling, A. Kusoglu, C. J. Radke, A. Z. Weber, Theory of multicomponent phenomena in cation-exchange membranes: Part I. Thermodynamic model and validation. J. Electrochem. Soc. 167, 013547 (2020).
- G. M. Geise, D. R. Paul, B. D. Freeman, Fundamental water and salt transport properties of polymeric materials. *Prog. Polym. Sci.* 39, 1–42 (2014).
- E. R. Nightingale, Phenomenological theory of ion solvation. Effective radii of hydrated ions. J. Phys. Chem. 63, 1381–1387 (1959).
- M. Tahaikt et al., Comparison of the performances of three commercial membranes in fluoride removal by nanofiltration. Continuous operations. *Desalination* 225, 209–219 (2008).
- L. A. Richards, B. S. Richards, B. Corry, A. I. Schäfer, Experimental energy barriers to anions transporting through nanofiltration membranes. *Environ. Sci. Technol.* 47, 1968–1976 (2013).
- C. K. Diawara et al., Influence of chloride, nitrate, and sulphate on the removal of fluoride ions by using nanofiltration membranes. Sep. Sci. Technol. 40, 3339–3347 (2005).
- X. Zhou et al., Intrapore energy barriers govern ion transport and selectivity of desalination membranes. Sci. Adv. 6, eabd9045 (2020).
- R. Epsztein, E. Shaulsky, N. Dizge, D. M. Warsinger, M. Elimelech, Role of ionic charge density in donnan exclusion of monovalent anions by nanofiltration. *Environ. Sci. Technol.* 52, 4108–4116 (2018).
- S. U. Hong, R. Malaisamy, M. L. Bruening, Separation of fluoride from other monovalent anions using multilayer polyelectrolyte nanofiltration membranes. *Langmuir* 23, 1716–1722 (2007).
- Y. Li, T. Xu, Permselectivities of monovalent anions through pyridine-modified anionexchange membranes. Separ. Purif. Tech. 61, 430–435 (2008).
- R. Epsztein, E. Shaulsky, M. Qin, M. Elimelech, Activation behavior for ion permeation in ion-exchange membranes: Role of ion dehydration in selective transport. *J. Membr.* Sci. 580, 316–326 (2019).
- T. Xu, Z. Liu, W. Yang, Fundamental studies of a new series of anion exchange membranes: Membrane prepared from poly(2,6-dimethyl-1,4-phenylene oxide) (PPO) and triethylamine. J. Membr. Sci. 249, 183–191 (2005).
- J. D. Moon, B. D. Freeman, C. J. Hawker, R. A. Segalman, Can self-assembly address the permeability/selectivity trade-offs in polymer membranes? *Macromolecules* 53, 5649–5654 (2020)